# The Influence of Layer Outcropping on the Separation of Boundary Currents. Part II: The Wind- and Buoyancy-Driven Experiments

ERIC P. CHASSIGNET, RAINER BLECK, AND CLAES G. H. ROOTH

*RSMAS/MPO, University of Miami, Miami, Florida*

(Manuscript received 18 November 1994, in final form 1 May 1995)

ABSTRACT

It is shown that the main characteristic of the Parsons western boundary current separation mechanism, namely a separation south of the zero wind stress curl line (ZWCL), is no longer present when diabatic effects are included through the addition of a mixed layer to the model structure. When diabatic processes are taken into account, the separation is associated with the outcropping of interior layers into the mixed layer where the horizontal density gradient is a maximum. The maintenance of this maximum results from a balance between potential vorticity conservation and diabatic processes. In spite of wide variations in either forcing functions or parameters, the flow patterns of the thermally forced experiments described herein remain very similar from one experiment to the other, with a separation latitude located at the ZWCL. It is only when salinity is allowed to vary significantly in space that one observes a significant move in the jet separation latitude.

## 1. Introduction

In Chassignet and Gent (1991) and Chassignet and Bleck (1993, referred to hereafter as Part I), the separation latitude of the western boundary current in a numerical model was found to depend strongly upon the choice of vertical coordinate. In the case of vertical discretization in constant density layers (isopycnic coordinate), depth variations large enough to result in layer outcropping can occur, which, in the absence of diabatic effects, provides a simple mechanism for large deviations in jet separation latitude from the linear theory (Parsons 1969; Kamenkovich and Reznik 1972; Veronis 1973; Huang and Flierl 1987). As stated by Veronis (1981), separation ". . . *must necessarily include the surfacing of the thermocline (with a possible mixed layer at the surface)*".

In Part I of this paper, the impact of layer outcropping on western boundary current separation was investigated in a series of experiments with an *adiabatic* multilayer eddy-resolving numerical model. It was shown that layer outcropping moves the separation latitude to the south of the zero wind stress curl line (ZWCL). The separation latitude is dictated by the stratification choice, that is, the fixed amount of fluid in the layers, and by the parameterization of the wind-induced stress profile in the water column. It is important to assess the factors behind the separation process, as most existing realistic eddy-resolving North Atlantic simulations to date (Thompson and Schmitz 1989; Beckman et al. 1994) exhibit an overshooting Gulf Stream at Cape Hatteras.

In the oceanic surface layer, *diabatic* effects play a significant role. The depth over which the wind acts is time and space dependent and the amount of fluid in each layer varies significantly in time. The question then arises as to whether these aspects, neglected in the adiabatic experiments of Part I, become important in the separation mechanism associated with layer outcropping. In this paper (Part II), the influence of thermodynamics on midlatitude jet separation is investigated by merging a thermodynamically active mixed layer (Bleck et al. 1989, 1992) to the numerical model (Bleck and Boudra 1986) used for the purely wind-driven experiments of Part I. Models with an adiabatic interior structure augmented by a dynamically and thermodynamically active surface mixed layer are attractive as they break the constraint of constant layer volume implicit in the adiabatic model and facilitate a dynamically more consistent representation of the vertical penetration of surface stress effects. Diapycnal effects are small in the main thermocline (Ledwell et al. 1993) and, to a first approximation, can be neglected on decadal timescales.

The layout of the paper is the following. In section 2, the adiabatic outcropping mechanism is discussed in relation to observations and diabatic effects. Section 3 introduces the diabatic version of the model. The "base" experiment is then presented and discussed in detail in section 4. Section 5 investigates the sensitivity

*Corresponding author address:* Dr. Eric P. Chassignet, Rosenstiel School of Marine and Atmospheric Science, Division of Meteorology and Physical Oceanography, University of Miami, 4600 Rickenbacker Causeway, Miami, FL 33149-1098.
E-mail: eric@akee.rsmas.miami.edu

of the midlatitude jet separation to changes in the thermodynamic forcing and to external parameters. In section 6, the importance of varying salinity (held constant in the cases of sections 4 and 5) is investigated. Finally, the results are summarized and discussed in the concluding section.

## 2. The adiabatic outcropping mechanism

In the models of Parsons (1969), Kamenkovich and Reznik (1972), Veronis (1973), and Huang and Flierl (1987), the ocean thermocline structure is represented by two immiscible layers with a specified amount of water in the upper layer. When the amount of warm upper-layer water is reduced below a critical value, the lower layer outcrops and the jet associated with the surfacing line resembles the Gulf Stream system. The assumptions behind these models are 1) immiscible layers, 2) a finite amount of water in the upper layer, and 3) the wind stress prescribed as a body force over the upper layer only. In a series of purely wind-driven (adiabatic) experiments (Part I), the separation latitude was shown to be dictated by 1) the parameterization of the wind-induced stress profile in the water column and 2) the stratification choice, that is, the fixed amount of fluid in the layers. Good agreement with observations can be obtained by a proper choice of wind stress and upper-layer volume (Gangopadhyay et al. 1992).

While assumption 3 above is acceptable as long as the forced upper-layer thickness is large compared to the Ekman depth, layer outcropping leads to a discontinuity in forcing that has been shown to be of extreme importance in the Parsons (1969) jet separation mechanism, as illustrated by the multilayer experiments of Part I. Temporal and spatial discontinuities in forcing appear as layers outcrop and the resulting circulation is highly sensitive to the stratification choice, that is, the somewhat arbitrary discretization of the continuous density field. In the ocean, however, the depth over which the wind acts is finite, time and space dependent, and is usually assumed to be the depth of the mixed layer. This problem can be alleviated as in Part I by replacing the discrete forcing mode by a formulation that provides a gradual transition in wind forcing as layers outcrop, that is, by defining a wind stress profile that decreases from a value $\tau_0$ at the surface to zero at some specified depth $d_{\max}$ representing observed mixed layer depth. These ad hoc assumptions, while of interest when exploring model sensitivity, are a poor representation of the processes at work.

The question as to whether the nature of Parsons's (1969) adiabatic solution, namely separation associated with the outcrop south of the ZWCL, is preserved in the presence of surface cooling/warming was addressed analytically by Pedlosky (1987) and by Nurser and Williams (1990). They showed that the presence of cross-isopycnal flows at the outcrop of the thermocline (corresponding to a conversion between light and abyssal waters (Veronis 1976) does indeed affect the flow pattern. In the case of moderately strong mass conversion (i.e., a "leaky" Ekman-layer flow), Pedlosky (1987) argued that the outcrop of the thermocline might no longer be associated with a detached boundary current. Nurser and Williams (1990) actually showed that heating along the outcrop line weakens the separating boundary current and shifts its path northward. They showed Pedlosky's solution to be a special limit of maximum possible heating. On the other hand, realistic cooling results in a strengthening of the boundary current and a southward shift of its separation point.

The impact of cross-isopycnal flows on the outcrop was investigated in a preliminary numerical calculation to confirm its importance to the separation process. The model configuration is the same as in Part I, namely a square, flat-bottom ocean basin (2000 km × 2000 km × 5 km) driven by a zonally symmetric wind stress $\boldsymbol{\tau} = [-\tau_m \cos(2\pi y/L), 0]$, with $\tau_m/\rho = 1 \times 10^{-4}$ m$^2$ s$^{-2}$ specified as a body force acting only on the layer directly beneath the surface. The horizontal grid is uniform with a spacing of 20 km. The vertical discretization consists of two layers, one thin (150 m) and the other relatively thick (4850 m). Nonlinearity associated with layer depth changes is included, but the inertial terms in the momentum equations are omitted. The upper-layer thickness field after 10 years of integration is shown in Fig. 1a for the experiment with no net flow across the outcrop line. The outcrop region (i.e., the region from which the layer has withdrawn) spans virtually all of the cyclonically forced region and extends into the anticyclonically forced region as well. The flow pattern is in fair agreement with the analytical solution (Part I; Sun et al. 1993).

The surface cooling or heating is mimicked as in Nurser and Williams (1990) by a net mass transfer between the two layers, applied across the frontal zone defined by the outcrop. This transfer, as discussed by Veronis (1976, 1978), corresponds to a conversion between light and abyssal waters and is given by an interfacial flux per unit length $U_c$ along the outcrop. Numerically, in this study, the transfer is achieved by specifying a mass conversion across the front associated with the outcrop, from the surface to a depth of 100 m (Fig. 1b). The return flow needed to conserve mass in each layer is prescribed over a thin band 60 km wide at the southern boundary. Four experiments were integrated until a steady state was reached: two with cooling and heating along the outcrop line as shown in Fig. 1b and two with cooling and heating applied only along the first 1000 km of the outcrop line. The specified interfacial flux is 2 Sverdrups (Sv $\equiv 10^6$ m$^3$ s$^{-1}$) per 1000 km and corresponds to a heat loss/gain of 200 W m$^{-2}$. The upper-layer thickness fields for these four experiments are displayed in Fig. 2.

As in Nurser and Williams (1990), the separation process is found to be quite robust to a moderate mass conversion and the flow pattern is not strongly modified

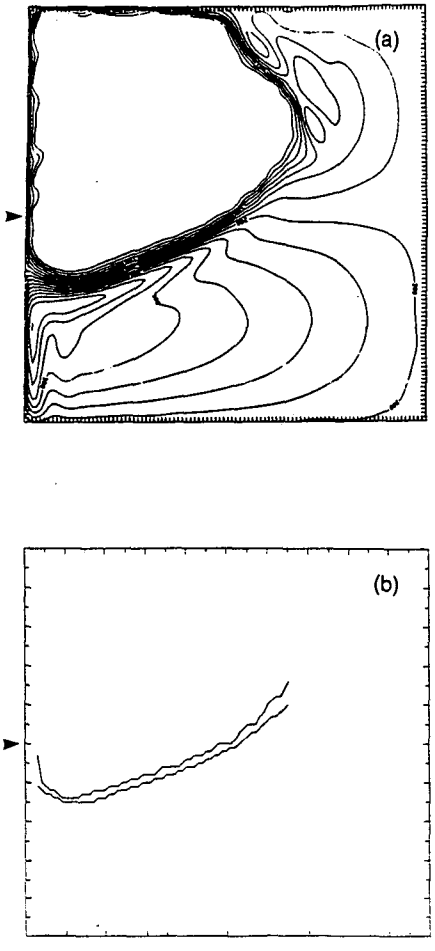


FIG. 1. (a) Upper-layer thickness field after 10 years of integration for the two-layer model with a contour interval of 25 m; (b) frontal zone associated with outcrop from the surface to a depth of 100 m. The arrow indicates the ZWCL.

when compared to the experiment with no net flow across the outcrop line (Fig. 1a). As in the analytical solution, the midlatitude jet separation latitude is observed to move south when cooling is prescribed [240 and 120 km, respectively (Figs. 2a,b)] or north in the case of heating [100 and 60 km, respectively (Figs. 2c,d)]. A good agreement was obtained between the numerical and analytical results, namely a southward (northward) displacement of the separation when cooling (heating) is prescribed. The question then arises as to whether this result holds up when the water mass transfer is achieved, through a mixed layer overlying the isopycnic layers, in response to the surface forcing.

In the experiments described in Part I and in this section, the separation associated with the outcropping mechanism is found to be dependent upon choices in the model configuration and formulation such as the amount of fluid in each layer, the mass transfer between layers, and the vertical distribution of the wind stress. For a realistic representation of the processes at work, one must then take into account the fact that 1) the amount of fluid present in the thermocline results from a complex thermodynamic balance and 2) the depth over which the wind acts is time and space dependent (the assumed depth of the mixed layer). By adding thermodynamic forcing and mixed layer physics, not only is the amount of fluid in each layer then allowed to vary as a function of the surface forcing, but the ambiguities associated with distributing the wind forcing over various layers are also removed. In the remainder of this paper, the influence of thermodynamics on the midlatitude jet separation mechanism of Parsons (1969) is therefore investigated by merging a thermodynamically active mixed layer (Bleck et al. 1989, 1992) to the numerical model (Bleck and Boudra 1986) used for the purely wind-driven experiments of Part I.

## 3. The numerical model

The primitive equation, pure-isopycnic model of Bleck and Boudra (1986) may be viewed as a stack of shallow-water models, each consisting of a momentum and a continuity equation:

$$\frac{\partial \mathbf{v}}{\partial t} + \frac{1}{2}\nabla_\rho \mathbf{v}^2 + (\zeta + f)\mathbf{k} \times \mathbf{v} = -\nabla_\rho M + Ah^{-1}\nabla_\rho \cdot h\nabla_\rho \mathbf{v} - \mu \mathbf{v}, \quad (1)$$

$$\frac{\partial h}{\partial t_\rho} + \nabla_\rho \cdot (\mathbf{v}h) = 0, \quad (2)$$

where $\zeta = v_x - u_y$ is the relative vorticity; $M = gz + p\alpha$ is the Montgomery potential; $h$ is the thickness of a layer of constant density; $\alpha = \rho^{-1}$ is the corresponding specific volume; $A$ is the lateral viscosity; and the bottom drag coefficient $\mu$ is zero except in the bottom layer. The subscript $\rho$ indicates derivatives on surfaces of constant density. Horizontal velocities and vorticity are defined as layer properties, while pressure and geopotential are defined at the interfaces between layers.

The merging of a thermodynamically active Kraus–Turner type mixed layer to the isopycnic layers is described in detail in Bleck et al. (1989) and Bleck et al. (1992). The equations solved in the mixed layer differ from the above set in three respects: (i) the horizontal pressure term becomes $-(\nabla M + p\nabla\alpha)$ to account for the fact that the mixed layer is nonisopycnic, (ii) a wind stress term is added, and (iii) an entrainment/detrainment rate is accounted for. The model also accomodates two thermodynamic variables, temperature $T$ and salinity $S$, varying independently in the mixed layer but dependent on each other in the isopycnic interior layers where $T$ is treated as a function of $S$ and $\rho$. For details, the reader is referred to Bleck et al. (1989, 1992) and Bleck and Chassignet (1994). The

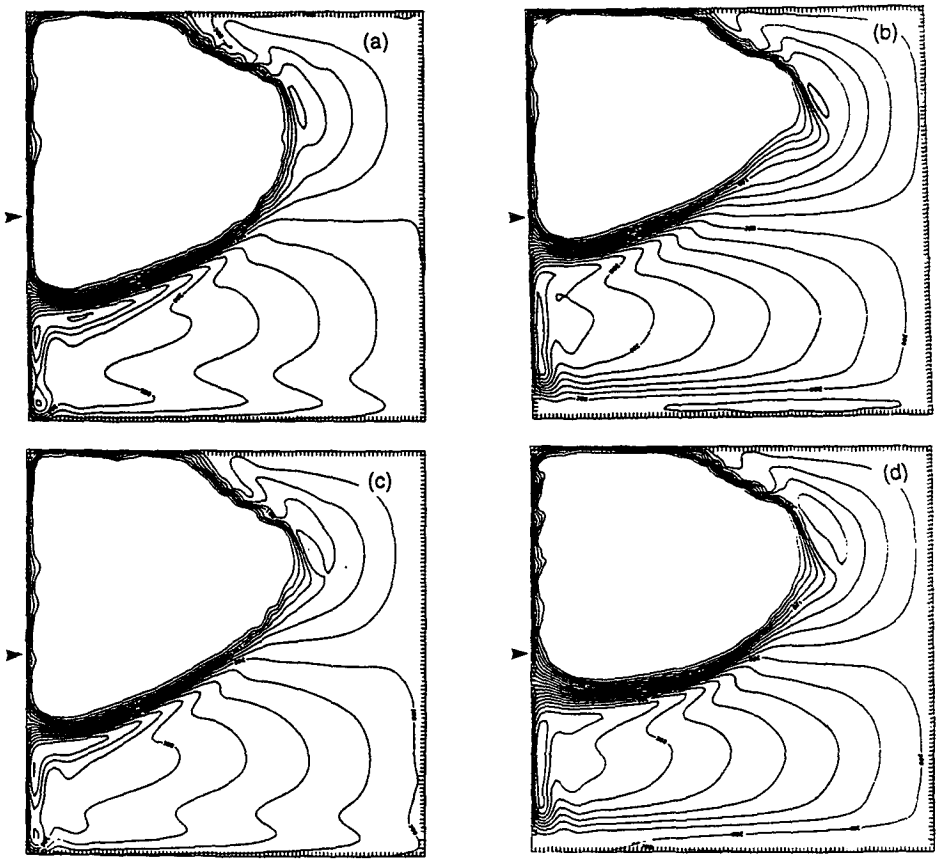


FIG. 2. As in Fig. 1a but with (a) cooling applied along the frontal zone of Fig. 1b; (b) as in (a) for heating; (c) cooling along the first 1000 k; (d) as in (c) for heating. The contour intervals are 25 m in (a) and (c) and 20 m in (b) and (d). The arrow indicates the ZWCL.

interior layers are set in motion by pressure torques and by bulk momentum transfer during mixed layer detrainment. A good depiction of subduction and thermocline ventilation processes is obtained in the model in the sense that a clear distinction exists between the mixed layer and the interior layers at all times at every grid point. Intersections of the moving coordinate surfaces with boundaries, such as the mixed layer boundary (outcropping), are handled by Smolarkiewicz's (1984) MPDATA scheme. This method combines the smoothness properties of the positive-definite upstream differencing scheme with the accuracy of space-centered schemes and controls the tendency to generate negative layer thickness when solving the layer thickness prediction equation. This approach has proven very effective [see Sun et al. (1993) for a review].

### *a. Model configuration*

The model configuration is designed to be a natural follow-up to the six-layer adiabatic experiment I3 of Part I. This experiment (I3) exhibits the principal characteristic of the two-layer experiment discussed in section 2, namely a separation south of the zero wind stress curl. The main reason for focusing on the six-layer experiment is that several interior isopycnic layers are needed for a good representation of the mixed layer entrainment/detrainment process (Bleck et al. 1989). The initial vertical spacing is, as in I3 (Table 1), nonuniform with greater resolution near the surface, except that the uppermost layer is now the thermodynamically active mixed layer. The domain corresponds to a square ocean basin (2000 km × 2000 km × 5 km). The horizontal grid is uniform with a spacing of 20 km. The circulation is damped by a small linear bottom drag and by lateral eddy viscosity, either deformation dependent or constant. The lateral boundary conditions employed on the four sidewalls are in general free slip, unless explicitly stated otherwise. The parameters for the experiments are given in Table 1.

### *b. Forcing functions*

The surface boundary conditions required to drive the mixed layer are the surface wind speed, the radiative fluxes, the sensible and latent heat fluxes, and in

TABLE 1. Parameters and forcing functions of the experiments.

| Experiment | Initial layer thickness (m) | $\sigma_\theta$ | Lateral dissipation ($m^2\ s^{-1}$) | Thermodynamic forcing functions |
|---|---|---|---|---|
| I3 | 50 | 25.7 | 400 | none |
| | 50 | 26.1 | Free slip | |
| | 200 | 26.5 | | |
| | 400 | 26.9 | | |
| | 800 | 27.3 | | |
| | 3500 | 27.7 | | |
| Base | | | | SHF1, SWS1, $E - P = 0$ |
| S1 | | | | SHF2, SWS1, $E - P = 0$ |
| S2 | | | | SHF1, SWS2, $E - P = 0$ |
| S3 | | | 200 | SHF1, SWS1, $E - P = 0$ |
| | | | Free slip | |
| S4 | | | 400 | |
| | | | No slip | |
| S5 | | | 400 | SHF1, SWS1, $E - P = f(y)$ |
| | | | Free slip | |
| S6 | | | | SHF1, SWS1, $E - P = 4 \times f(y)$ |
| S7 | | | | SHF1, SWS1, $E - P = -f(y)$ |

For all experiments, the linear bottom drag is $5 \times 10^{-8}\ s^{-1}$. The function $f(y)$ is equal to $-10^{-6}y$ (m $yr^{-1}$) with $y$ in meters (zero at the ZWCL). Blanks indicate no change from the previous experiment.

one experiment, the freshwater flux. The wind stress, as in the adiabatic experiments of Part I, is zonally symmetric and is expressed as $\boldsymbol{\tau} = [-\tau_m \cos(2\pi y/L), 0]$, where $\tau_m/\rho = 1 \times 10^{-4}\ m^2\ s^{-2}$. The direct effect of the wind forcing is assumed not to extend past the bottom of the mixed layer. The resulting Sverdrup gyre circulation is antisymmetric with a counterclockwise gyre north of the wind stress curl zero and a clockwise gyre to the south.

The surface heat flux is expressed in terms of air–sea temperature differences (Haney 1971; Han 1984; Bleck et al. 1989) parameterized as $Q(T - T^*)$ where $T$ is the sea surface temperature and $Q$ and $T^*$ are parameters that vary in time and space. They are derived either, as in Bleck et al. (1989), from Lamb and Bunker (1982) and the Comprehensive Ocean–Atmosphere Data Set (COADS) (hereafter referred to as SHF1), or, as in Han (1984), from "various sources" (sic) (hereafter referred to as SHF2).

The surface wind speed needed to estimate the turbulent kinetic energy production due to mechanical stirring and bulk surface fluxes is derived either, as in Bleck et al. (1989), from COADS and varies with time and latitude (hereafter referred to as SWS1), or is constant in time as a function of the wind stress (hereafter referred to as SWS2). Finally, freshwater flux, or "$E - P$" (evaporation minus precipitation) is, as in Bleck et al. (1992), patterned after Schmitt et al. (1989) and modified for zero net freshwater production.

The forcing functions correspond to a 2000 km $\times$ 2000 km North Atlantic area centered at 35°N. One must keep in mind that the wind stress profile is idealized and constant in time. This is not consistent with the choices made for the other forcing functions that are based on observations (except for SWS2) and that vary both in space and time. This combination was chosen to obtain a mixed layer depth cycle with constant wind stress to provide a meaningful comparison with the adiabatic experiment of Part I. The work presented here should therefore be considered a process study aimed at understanding the impact of mixed layer physics/thermodynamics on midlatitude jet separation in an idealized setting. Table 1 lists the forcing functions used in each experiment.

## 4. The "base" experiment

As noted in the previous section, the model configuration is designed to be a natural follow-up to the six-layer adiabatic experiment I3 of Part I. In the base experiment, salinity is held constant at 34.5 mil, and for the five $\sigma_\theta$ values of the underlying layers (Table 1), the corresponding temperatures are 13.0°, 10.7°, 8.1°, 4.8°, and −0.4°C. The surface forcing functions are SHF1 and SWS1 (Table 1). In order to accelerate the spinup of the basin circulation, a zonally symmetric density structure derived from Levitus (1982) is initially imposed. Mechanical spinup is achieved after 5 years of integration.

The main objective of this section is to describe the evolution of the diabatic processes in the upper layers in response to the annual growth and retreat of the mixed layer, in comparison to the six-layer adiabatic experiment I3 of Part I. Figure 3 illustrates the annual cycle of the mixed layer temperature (Figs. 3a,b), depth (Figs. 3c,d), and corresponding surface heat flux fields (Figs. 3e,f) in the 10th year of integration. In both the cool (March) and warm (September) seasons, the temperature contrast between the subpolar and sub-

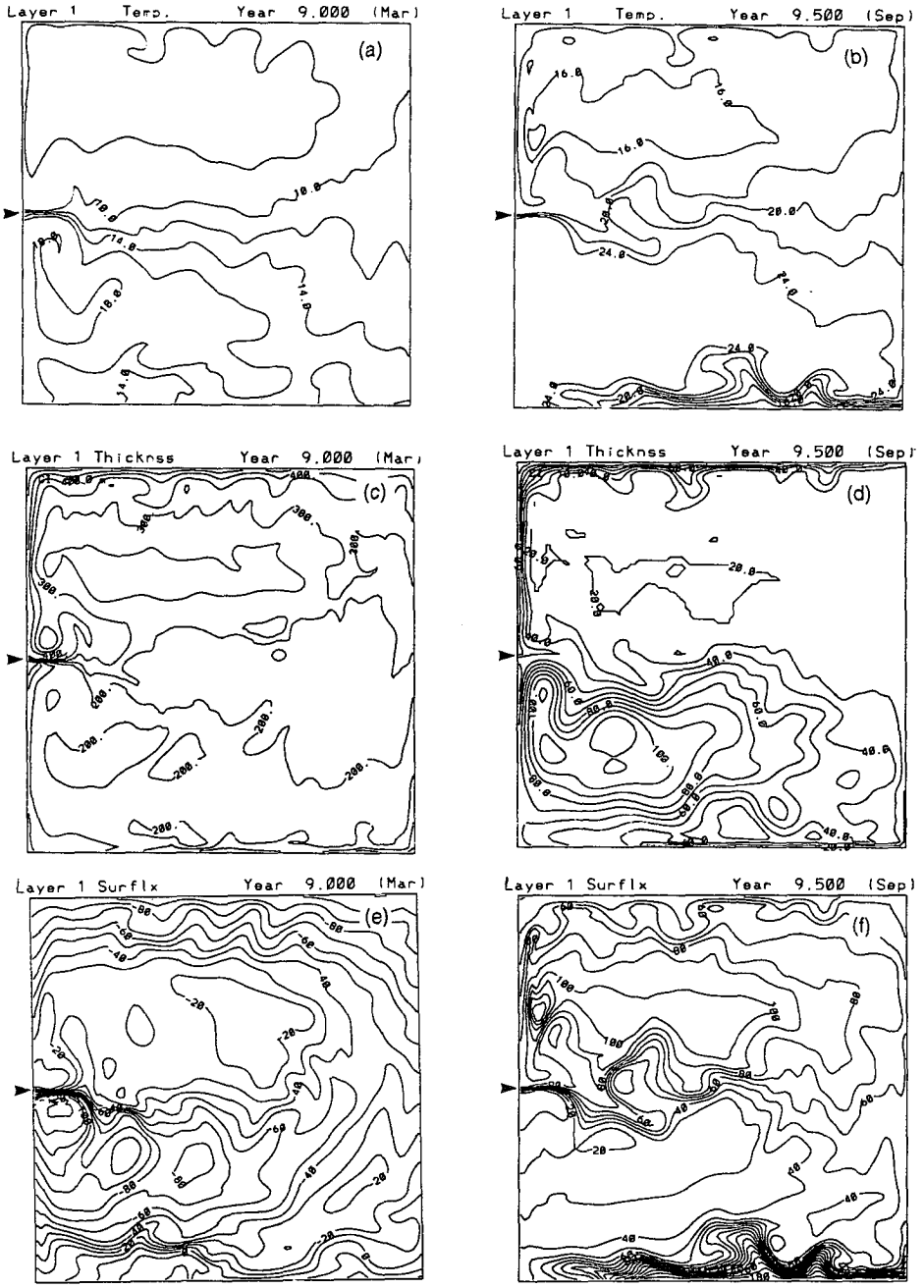


FIG. 3. Base experiment: (a, b) mixed layer temperature (°C) in March and September of year 9; (c, d) mixed layer depth in March (contour interval, 100 m) and in September (contour interval, 10 m); (e, f) surface heat flux (W $m^2$) in March and September. The arrow indicates the ZWCL.

tropical gyres is of the order of 10°C, but the averaged summer sea surface temperature (SST) is warmer than in winter by about 6°C. In September, strong upwelling is present at the southern boundary with signatures both in the mixed layer depth field and in the surface heat flux (Figs. 3d,f). The mixed layer is, as expected, shallow in summer (less than 20 m in the subpolar gyre and less than 100 m in the subtropical gyre) and deep in winter (up to 500 m in the subpolar gyre) (Figs. 3c,d). The surface heat flux (positive upward) is negative in winter and positive in summer with an amplitude of approximately 100 W $m^2$.

The annual growth/retreat of the mixed layer is best illustrated by vertical cross sections. The meridional

sections shown in Fig. 4 run 500 km north and south of the ZWCL, are 2500 m in depth, and are drawn at 100 km east of the western boundary. Only the annual extremes of the mixed layer advance (March) and retreat (September) are displayed. In March, three of the interior layers outcrop into the mixed layer at the front associated with the midlatitude jet and the separation between the subpolar and subtropical gyres. Only the two deepest layers ($\sigma_\theta$ = 27.3 and 27.7) cover the whole basin (Fig. 4a). In September, the mixed layer is very shallow (Figs. 3d, 4b) and the lower layers outcrop into the mixed layer in a manner similar to that of the adiabatic experiment I3. In that experiment, the isopycnals intersect the ocean surface (Fig. 8 of Part I).

The mass transport streamfunctions in each layer for the months of March and September are displayed in Figs. 5 and 6, respectively. By comparing these flow patterns to the ones from the adiabatic experiment I3 of Part I, one is able to assess the impact on the basin circulation of the mixed layer growth and retreat as well as of the difference in wind-forcing prescription. Except for the separation latitude of the jet, the flow patterns of the thermally forced experiment are in good agreement with the adiabatic patterns, particularly in September when the lower layers cover a similar area of the basin. Layer 4 ($\sigma_\theta$ = 26.9) covers only half the basin in March when it outcrops into the deep mixed layer. A difference worth noting is the presence of two recirculation cells on each side of the midlatitude jet in the thermally forced experiments versus only one such cell south of the jet in the adiabatic experiment (Chassignet 1995). The separation south of the ZWCL in the adiabatic experiment, characteristic of Parsons's (1969) mechanism, is moved north to exactly the ZWCL in the thermally forced experiment. There is no meridional variation in the position of the separation associated with the seasonal growth/retreat of the mixed layer.

In summary, the flow patterns of the thermally forced experiment are in good agreement with the adiabatic ones. The variations in mixed layer depth associated with the seasonal forcing do not modify drastically the interior layer flow patterns. The major differences appear to be in the separation latitude of the jet, now located at the ZWCL rather than south of it, and in the recirculation cells.

## 5. Sensitivity experiments—Constant salinity

The adiabatic experiment I3 of Part I was forced only by the wind stress field. Thermal forcing results in several additional degrees of freedom that must be taken into account. Of interest also is the sensitivity of the solution to internal parameters such as lateral boundary conditions and eddy viscosity. In this section, the importance of 1) the surface heat flux, 2) the surface wind speed, 3) the lateral boundary conditions, and 4) the eddy viscosity on the flow pattern are discussed in detail. As in the base experiment, salinity is held constant.

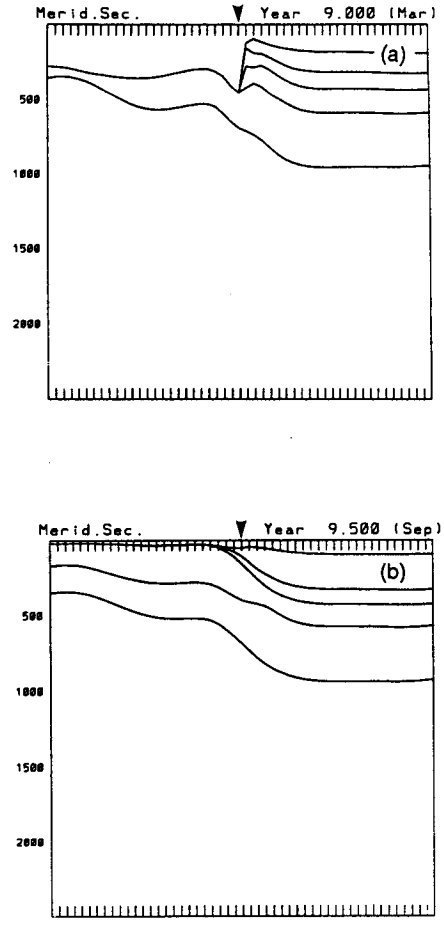


FIG. 4. Base experiment: meridional vertical cross sections drawn at 100 km east of the western boundary and centered at the ZWCL (arrow), for (a) March and (b) September. The meridional extent is 1000 km.

### *a. Sensitivity to the surface heat flux formulation—S1*

Experiment S1 is identical to the base experiment except for the surface heat flux that is now SHF2, with $Q$ and $T^*$ derived from Han (1984). For comparison, the distribution of $Q$ and $T^*$ over the basin from SHF1 (COADS data) and from SHF2 (Han 1984) are displayed in Figs. 7 and 8, respectively, for the months of March and September. SHF1 uses zonally averaged data while SHF2 varies also with longitude. Here $T^*$ is actually quite zonal in SHF2, but its range is greater (from 4° to 24°C in March and from 18° to 28°C in September) than in SHF1 (from 4° to 17°C in March and from 22° to 30°C in September). The difference is greater in winter in the southern part of the domain. A more significant difference is observed in $Q$, which is on the average two to three times larger in SHF2 than in SHF1. This results in faster temperature adjustment to seasonal fluctuations in S1 than in the base experiment. The resulting surface heat flux (Figs. 9c,d) is

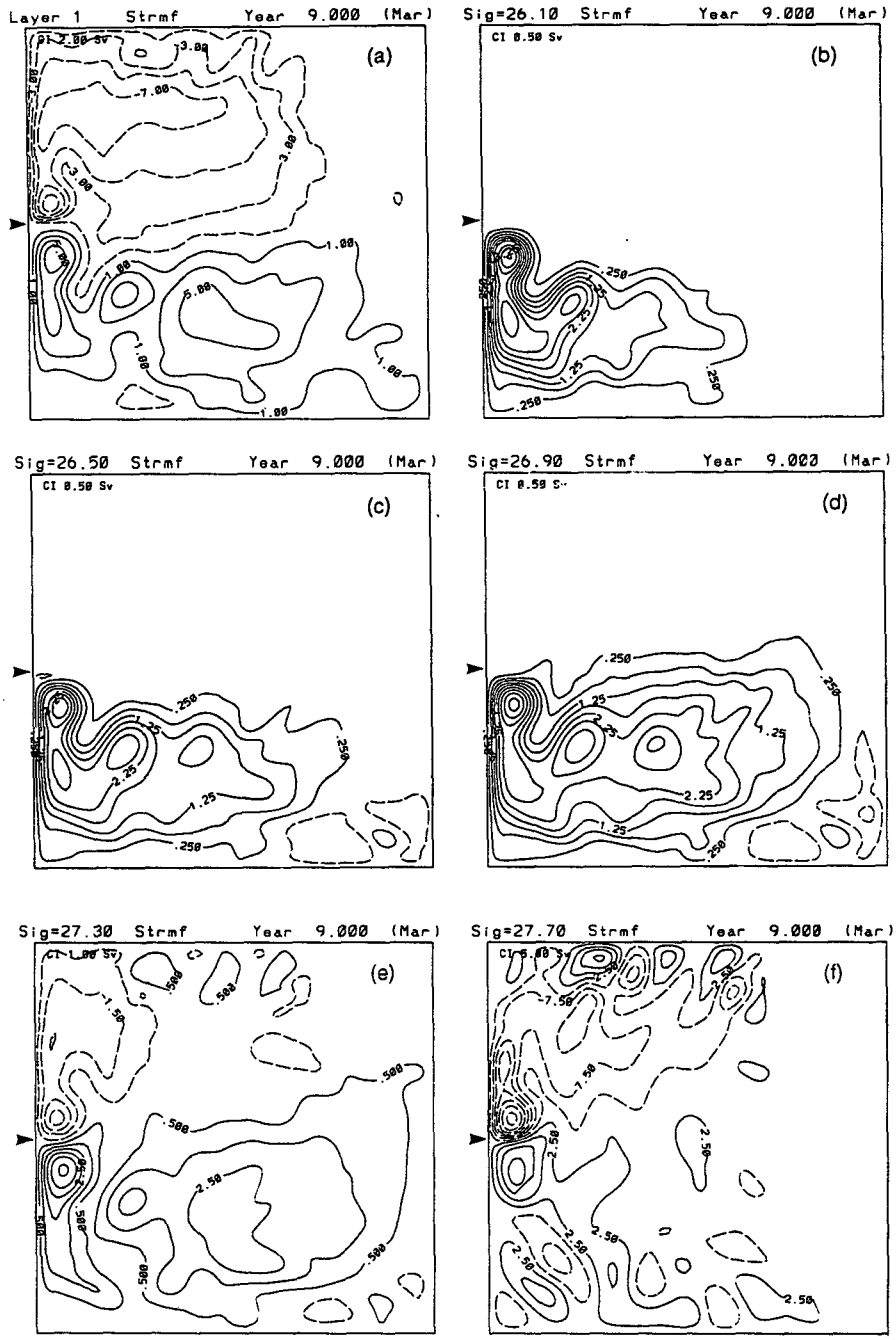


FIG. 5. Mass transport streamfunctions (Sverdrups) of the base experiment for each layer for the month of March. The arrow indicates the ZWCL.

therefore smaller on average than in the base experiment (Figs. 3e,f), and the mixed layer temperature field distribution is closer to $T^*$ (Figs. 7 and 9a,b) than in the base experiment (Figs. 3a,b).

The mixed layer growth/retreat cycle (Fig. 10) does not differ greatly from the base experiment (Fig. 4), except for an earlier retreat and deepening of the mixed layer by one month in S1. The turbulent kinetic energy input by the wind is the same in both experiments and the horizontal mixed layer depth distribution (not shown) is similar to that of the base experiment. The mass transport layer streamfunctions also do not differ greatly from the base experiment and are therefore not displayed. As in the base experiment, the midlatitude

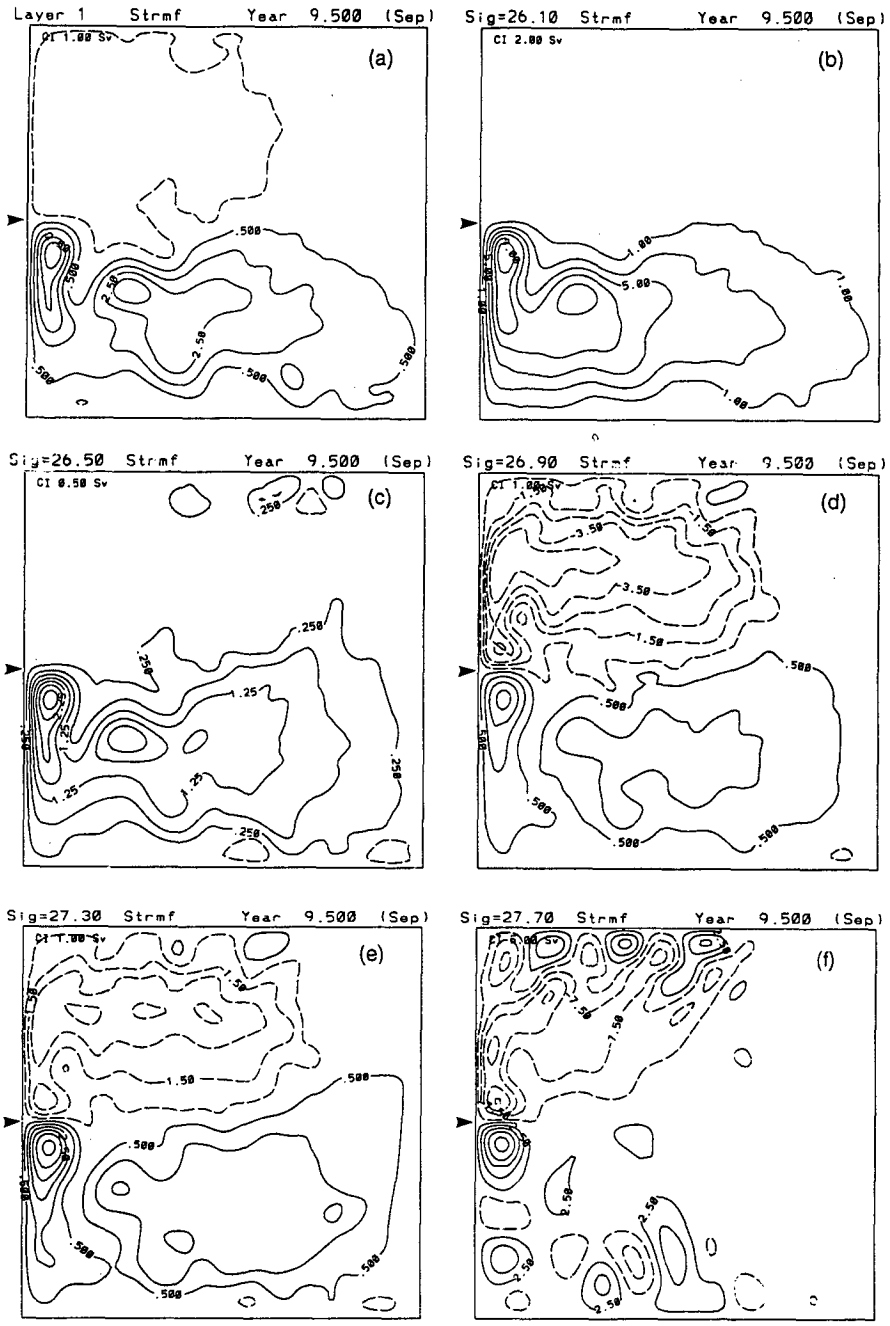


FIG. 6. As in Fig. 5 for the month of September.

jet separates at the ZWCL. In summary, a change in the surface heat flux does not modify the flow pattern despite a strong change in the sea surface temperature gradient.

### b. *Sensitivity to the surface wind speed formulation—S2*

In addition to the surface heat flux, one must specify a surface wind speed field that prescribes the turbulent kinetic energy input into the mixed layer. The wind speed also enters into the formulation of $Q$ and $T^*$ for SHF1 (Bleck et al. 1989). Instead of using a seasonally varying wind speed field derived from observations as in the base experiment (SWS1), S2 was forced by the surface heat flux SHF1 and by the surface wind speed SWS2 that corresponds directly to the wind stress (using a constant drag coefficient of $10^{-3}$). The field SWS2 has on the average a smaller magnitude than

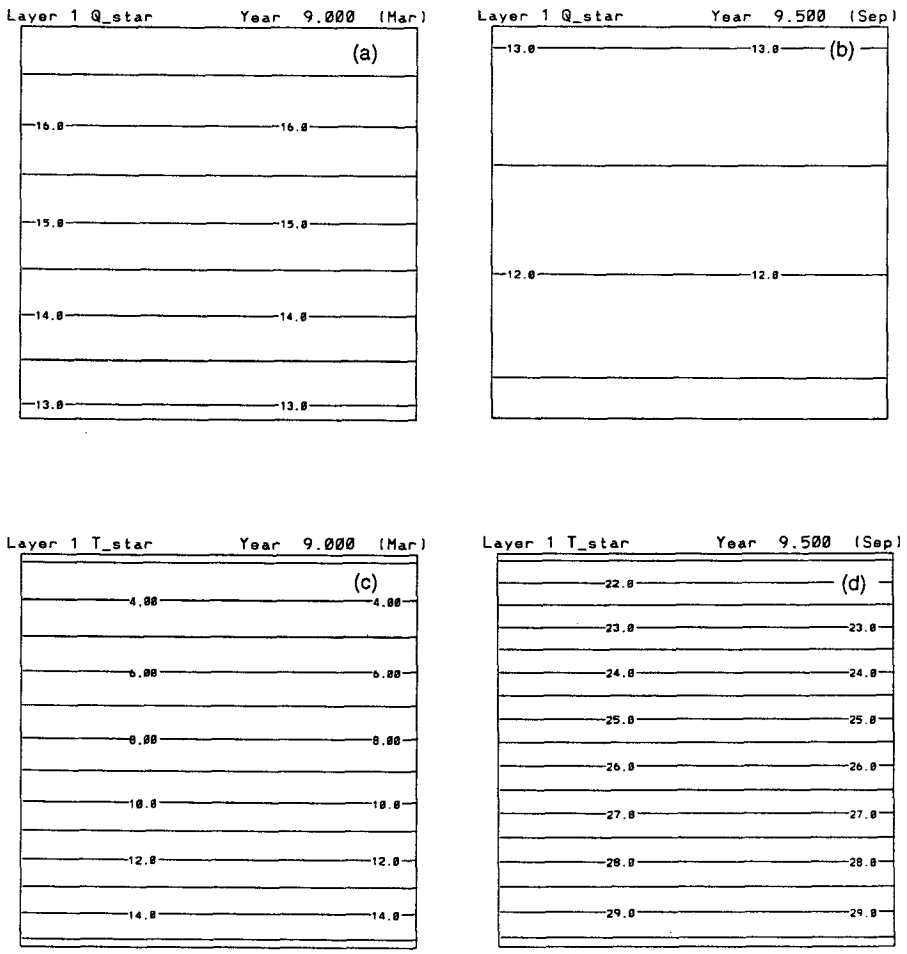


FIG. 7. Distribution of $Q$ (W m$^2$ K$^{-1}$) and $T^*$ (°C) from SHF1 (COADS data) for March and September, respectively.

SWS1. Consequently, the mixed layer growth/retreat cycle does not display the variability found in the base experiment, as illustrated in Fig. 11. The maximum mixed layer depth is only ~200 m versus 500 m for the base experiment (Fig. 4). A change in the wind speed does affect both the surface heat flux formulation and the turbulent kinetic energy input into the mixed layer. Despite this change, the mass transport layer streamfunctions of S2 (not displayed), like those of S1, do not differ greatly from the layer streamfunctions of the base experiment. The jet separation latitude remains located at the ZWCL.

### c. *Sensitivity to the lateral eddy viscosity coefficient—S3*

As discussed in the two previous subsections, the model solution appears to be quite stable to changes in the external forcing functions. In order to explore its sensitivity to internal parameters, first the magnitude of the lateral eddy viscosity coefficient is decreased to about half the value used in the base experiment (Table 1). This increases the nonlinearity of the solution and the circulation thus becomes more inertial. This has been shown to have a significant impact on the jet separation (Cessi 1991; Chassignet and Bleck 1993; Chassignet 1995).

The most striking difference between S3 and the base experiment is in the intensity of the recirculating gyres (Fig. 12). In both experiments, dissipation is achieved through the inertial gyres where potential vorticity is modified within the compressed streamlines (Cessi 1991). The recirculation transport reached 100 Sverdrups in S3 (Fig. 12b) versus 50 Sverdrups in the base experiment (Fig. 12a). As noted earlier, two recirculating gyres are present. This is not the case for the adiabatic experiments (Part I; Chassignet 1995) that display only one recirculating gyre south of the separation. Despite the increase in variability and fluctuations in the jet's position, the separation latitude remains on the average at the ZWCL.

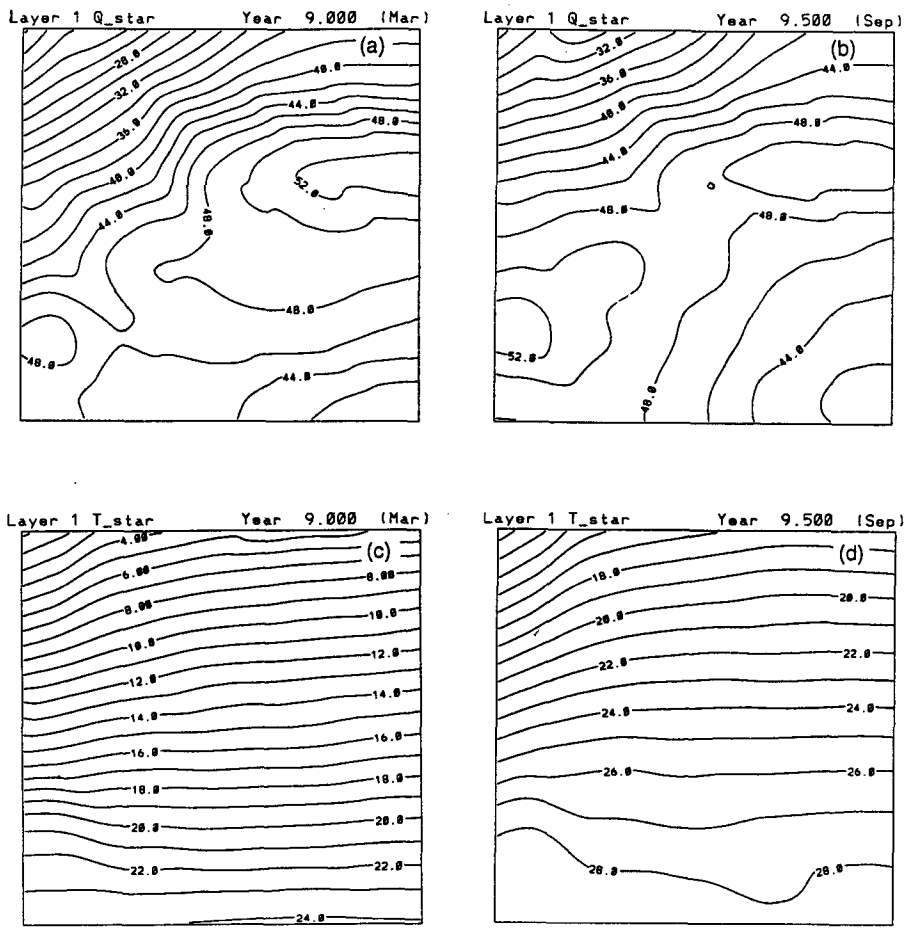


FIG. 8. As in Fig. 7 for SHF2 (Han 1984).

*d. Sensitivity to the lateral boundary condition—S4*

Midlatitude jet separation is sensitive to the choices made for the lateral boundary conditions (Cessi 1991; Chassignet and Gent 1991; Haidvogel et al. 1992; Chassignet 1995). In Haidvogel et al. (1992), the choice of no-slip lateral boundary conditions leads to an early separation of the midlatitude jet and the formation of a double "Gulf Stream." In contrast, the adiabatic outcropping mechanism discussed in Part I and in Chassignet (1995) is a large-scale response and is in principle independent of the choice made for the lateral boundary condition. This is true if the dissipation is achieved through inertial recirculating gyres (Chassignet 1995). Experiment S4 is identical to the base experiment, except that no-slip lateral boundary conditions are now prescribed on all boundaries.

There are no drastic changes in the circulation patterns between S4 and the base experiment. Small differences can be noted, such as the tendency for a more southerly jet detachment from the coast in the summer months. The western boundary current, instead of hugging the coast up to the ZWCL as in the base experiment, leaves the coast approximately 100 km south of the ZWCL. The sharp eastward turn, however, occurs at the ZWCL. The winter months do not exhibit this early detachment. This aspect is well illustrated by the density anomaly field displayed in Fig. 13. As in the adiabatic experiments, the choice of lateral boundary condition does not modify the flow pattern.

## 6. Variable salinity experiments

Despite significant changes in forcing or internal parameters introduced in the previous section, the midlatitude jet separation latitude remains at the ZWCL. As illustrated by Fig. 13, the midlatitude jet is associated with a large density contrast as warm and lighter water from the subtropical gyre is advected northward while cold and heavier water from the subpolar gyre moves southward. This is the point at which the underlying layers naturally outcrop into the mixed layer. Considering both the "mechanical" effects such as wind forcing and inertia and the "diabatic" effects such as surface heat and freshwater fluxes, one can ask which is more likely to affect the density distribution.

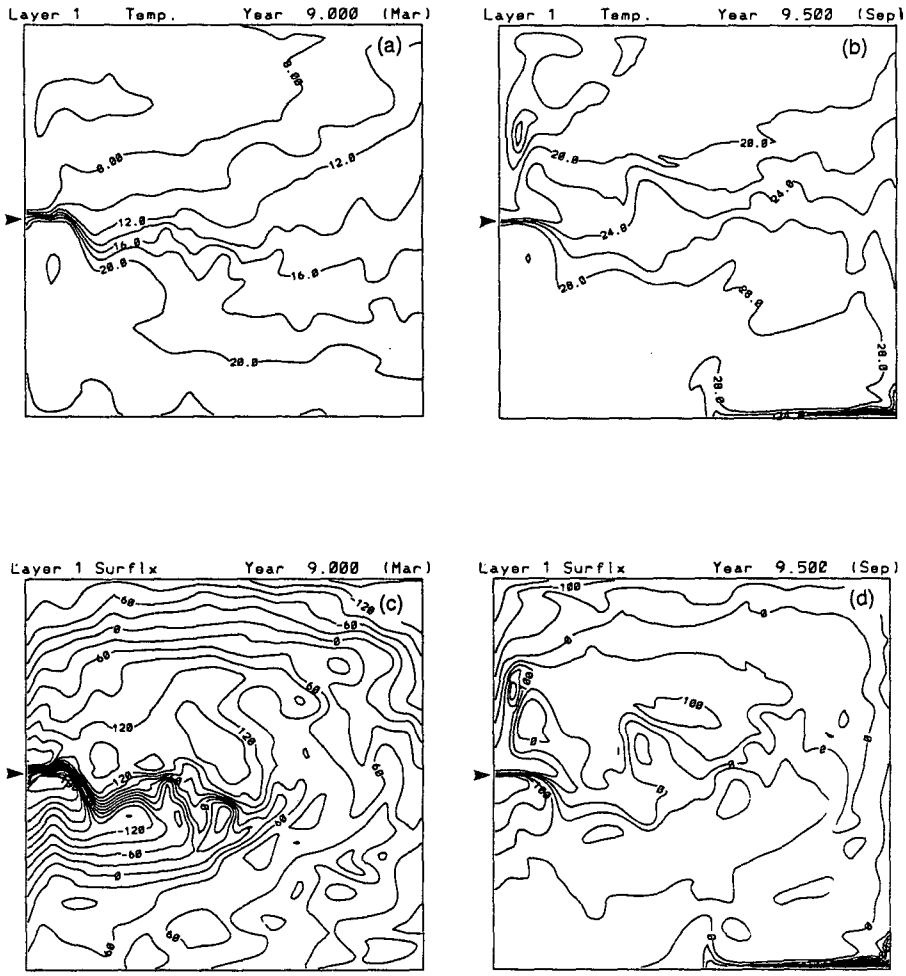


FIG. 9. Experiment S1: (a, b) mixed layer temperature (°C) in March and September of year 9; (c, d) surface heat flux (W $m^2$) in March and September. The arrow indicates the ZWCL.

The horizontal density gradient is maintained by a balance between the advection of warm (cold) water by the subtropical (subpolar) gyre and the thermodynamic forcing that modifies the background density field. The prescribed surface heat flux restores the sea surface temperature toward a $T^*$ (Figs. 7, 8), which maintains the temperature–density contrast between the two gyres. As illustrated by the previous sensitivity experiments, this balance appears to be quite robust when salinity is held constant. The prescription of a freshwater flux is able to affect this balance as illustrated in the remainder of this section.

In the following three experiments, S5, S6, and S7, the salinity is no longer held constant but is allowed to vary in time and space in each layer (Bleck et al. 1992). Following Bleck et al. (1992), the imposed freshwater flux, or $E - P$, is patterned after Schmitt et al. (1989), translated into a salinity flux, and finally modified for no net salt production. This yields $E - P$ values of the order of $\pm 1$ m $yr^{-1}$, positive in the subtropical gyre and negative in the subpolar gyre (Fig. 14 and Table 1). The zero value of $E - P$ is located at the ZWCL (35°N). The salinity flux is constant in time and makes the water lighter in the subpolar gyre and denser in the subtropical gyre, therefore reducing the density contrast between the two.

Experiment S5 is identical to the base experiment except that salinity is not fixed to 34.5 psu. The salinity and density fields and vertical cross sections are displayed in Fig. 15 for the months of March and September. The resulting salinity distribution varies from a high of 34.5 and a low of 34.1 in winter to a high of 34.8 and a low of 32.8 in summer (Figs. 15a,b). The solution has not yet reached complete equilibrium as the salinity gradient is slightly greater in March of the following year. The resulting density gradient between the northern and southern gyres is weaker both in summer and winter as shown in Figs. 15c,d. The net result is that fewer layers outcrop into the mixed layer, especially in summer when it is shallow (Figs. 15e, f).

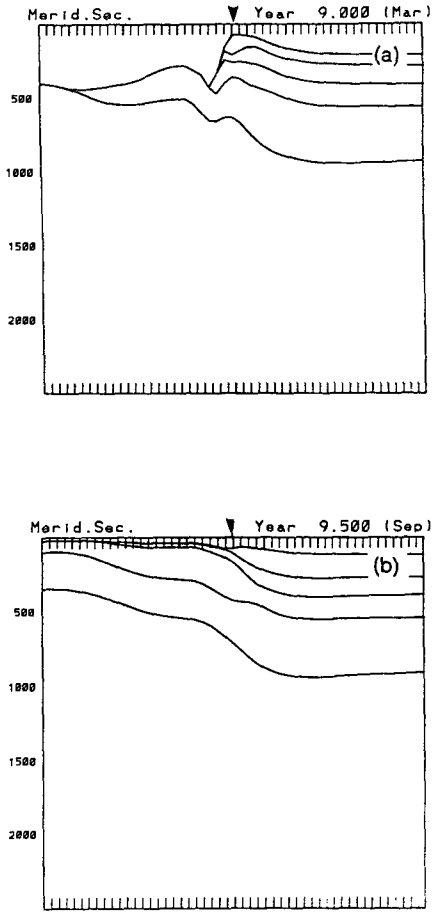


FIG. 10. As in Fig. 4 but for S1.

Again, as in the previous experiments, the midlatitude jet separates at the ZWCL.

To study an extreme case of freshwater flux and accelerate the model's response, S5 was further integrated for 5 years with an $E - P$ four times stronger basinwide (experiment S6). As for S5, the salinity and density fields and the vertical cross sections of S6 are displayed in Fig. 16 for the months of March and September. In S6, the resulting salinity gradient is much stronger (Figs. 16a,b) and the density gradient much weaker (Figs. 16c,d) than in S5. Even fewer layers outcrop into the mixed layer in winter than in S5 and none outcrop in summer (Figs. 16e, f). The resulting picture shows a jet separation latitude that has moved to 100 km north of the ZWCL (Figs. 16c,d). The flow pattern in each layer is otherwise similar to those of the base experiment.

Finally, experiment S7 was integrated, as S6, for a period of 5 years, but with an $E - P$ of the opposite sign. While this is an unrealistic scenario, the net effect is a strengthening of the density contrast between the two gyres. The impact on the separation, however, is minimal as it is again located at the ZWCL. The resulting salinity gradient is of the opposite sign (Figs. 17a,b) and the density gradient is much stronger (Figs. 17c,d) than in S6. Because of this stronger gradient, almost all of the upper layers outcrop into the mixed layer (Figs. 17e, f).

## 7. Discussion and concluding remarks

The experiments described in the previous sections were aimed at developing an understanding of the jet separation in large-scale diabatic eddy-resolving simulations in isopycnic coordinates. Without any diabatic effects, it was shown in Part I that the outcropping mechanism moves the midlatitude jet separation latitude to a point south of the ZWCL. Diabatic effects were included by merging a thermodynamically active mixed layer to the adiabatic numerical model used for the purely wind-driven experiments. In spite of wide variations in either forcing functions or parameters, the flow patterns of the diabatic experiments remain very similar from one experiment to the other. It is only when salinity is allowed to vary significantly in space

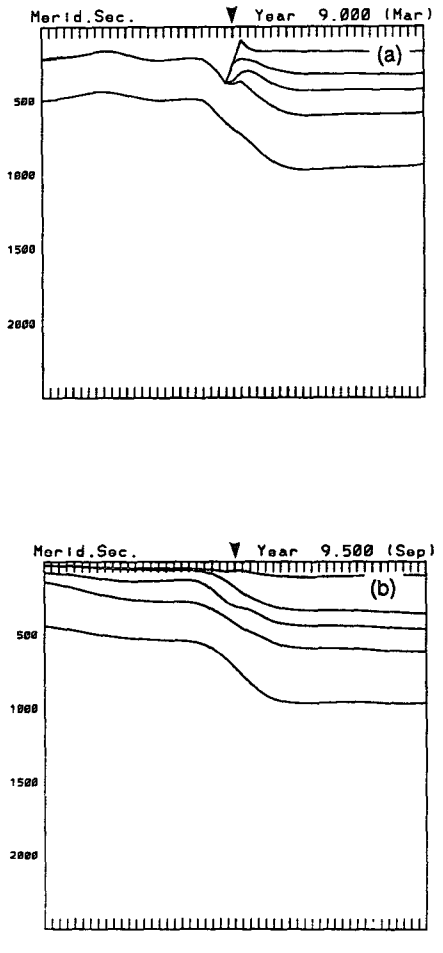


FIG. 11. As in Fig. 4 but for S2.

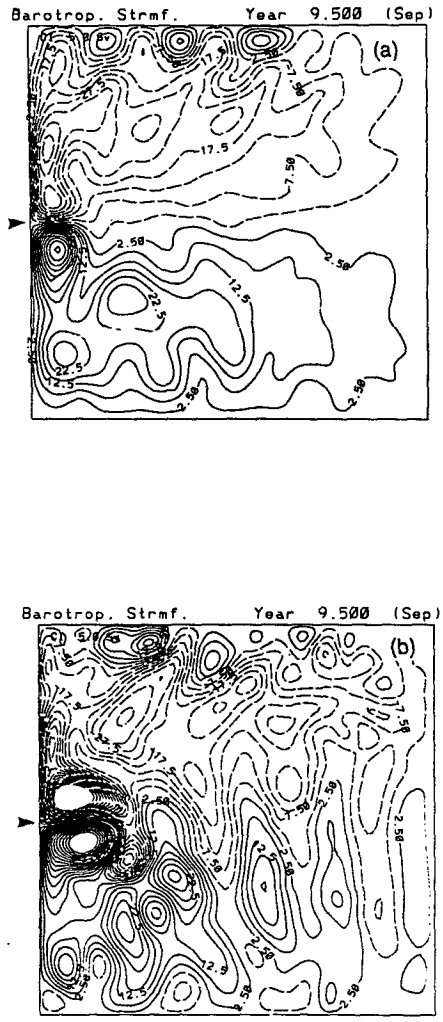


FIG. 12. Barotropic streamfunctions (Sverdrups) for the month of September in (a) the base experiment and (b) S3. The arrow indicates the ZWCL.

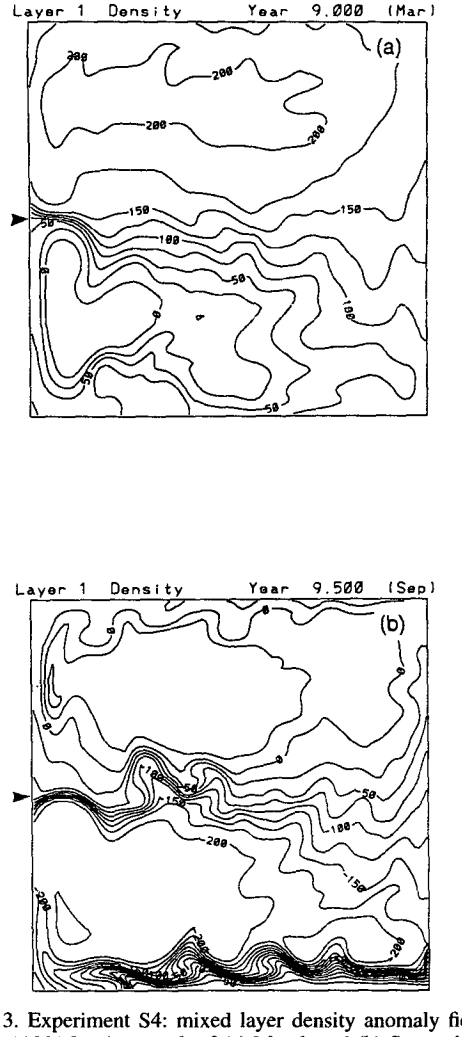


FIG. 13. Experiment S4: mixed layer density anomaly field [$(\sigma_\theta - 25) \times 1000$] for the month of (a) March and (b) September. The arrow indicates the ZWCL.

that a significant move in the jet separation latitude is observed.

In this discussion, one must bear in mind that the experiments have been performed in an idealized setting, namely a square basin (2000 km × 2000 km) driven by a zonally symmetric wind stress. Some of the results presented here are likely to change for an asymmetric forcing, as illustrated by Cessi (1991), Verron and LeProvost (1991), and Chassignet (1995). However, a symmetric wind stress does not necessarily imply a midlatitude jet separation at the ZWCL, as illustrated in Part I and Chassignet and Gent (1991). Depending on the model formulation and vertical discretization (quasigeostrophic, linear balance, or primitive equation in level or isopycnic coordinates), the midlatitude jet can either under- or overshoot the ZWCL when forced by a symmetric wind stress. It is by developing an understanding of the midlatitude jet

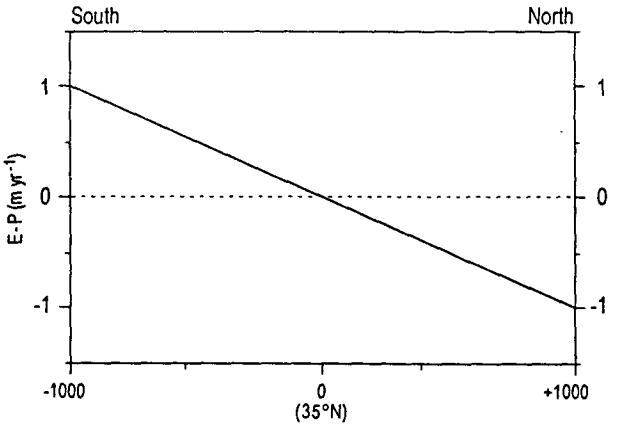


FIG. 14. Freshwater flux (m $yr^{-1}$) imposed in experiment S5.

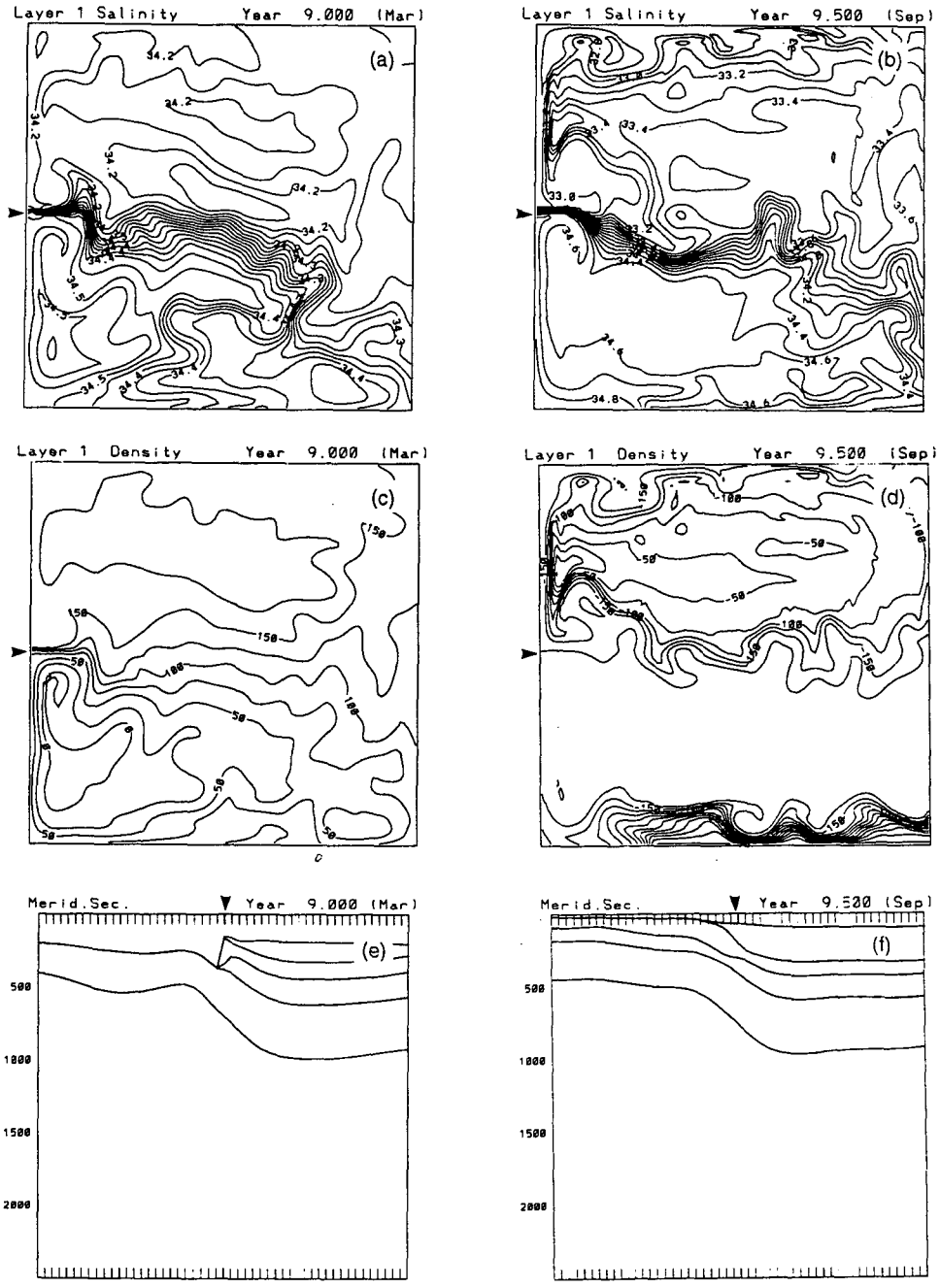


FIG. 15. Experiment S5: (a, b) salinity distribution in March and September; (c, d) mixed layer anomaly density field [$(\sigma_\theta - 25.) \times 1000$] in March and September; (e, f) vertical cross sections in March and September. The arrow indicates the ZWCL.

separation in this simplified setting that one will eventually be able to physically interpret more complex simulations.

The main characteristic of the Parsons (1969) separation mechanism, namely a separation south of the ZWCL, is no longer present when adiabatic effects are included through the addition of a mixed layer. Parsons's mechanism has been shown to be quite dependent upon the assumption of a wind stress acting as a body force on the isopycnic layer in contact with the atmosphere and upon the stratification choices. This assumption is relaxed with the addition of a nonisopycnic mixed layer, and, while the separation is still associated with interior layers outcropping into the mixed layer,

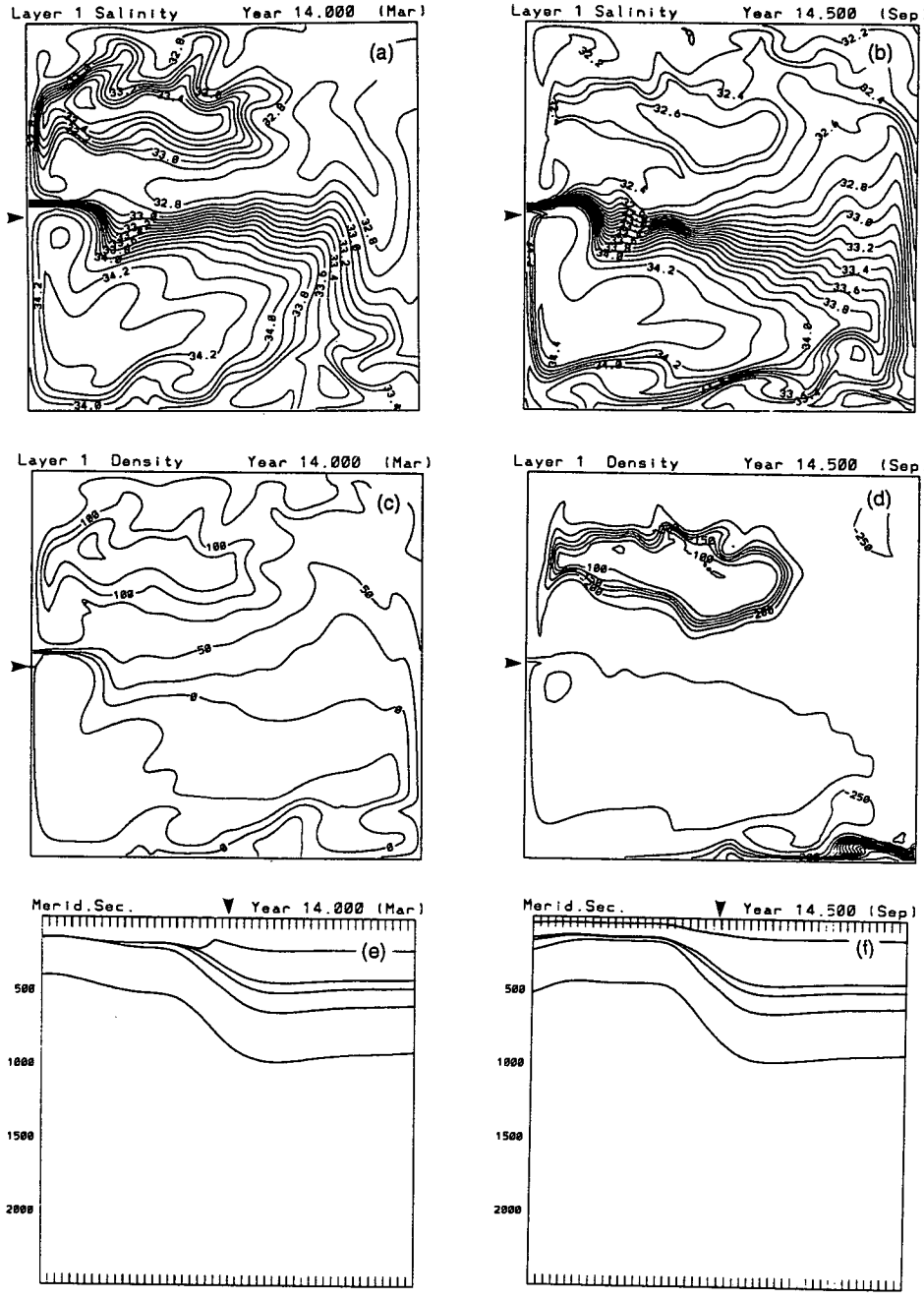


FIG. 16. As in Fig. 15 but for experiment S6.

it is no longer south of the ZWCL. This outcropping results from a balance between advection of water from the north and from the south and the imposed heat and freshwater fluxes. Advection is primarily controlled by the mechanical forcing (wind stress) and by the resulting circulation [given to first order by potential vorticity conservation arguments (Stommel 1960)]. In the experiments presented in this paper, the mechanical forcing appears to be dominant, as the separation latitude is quite insensitive to strong changes in thermodynamic forcing. It is only when the imposed freshwater flux is anomalously high that one can observe a northward movement of the separation latitude.

When an extreme freshwater flux was prescribed in experiment S6, a significant northward move of the separation latitude was observed in comparison to the base experiment. Since many uncertainties plague $E - P$ observations, the freshwater flux is often pre-

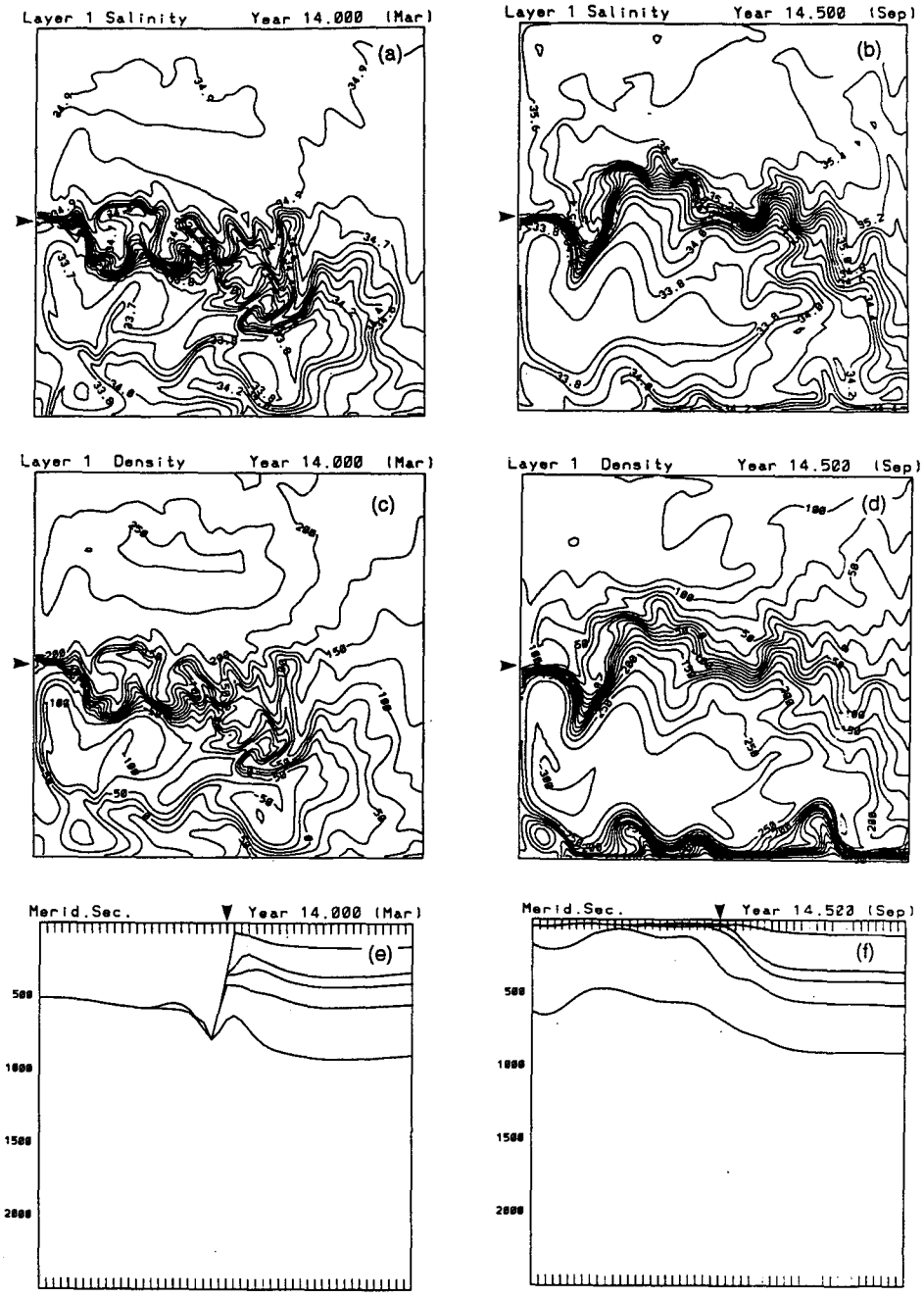


FIG. 17. As in Fig. 15 but for experiment S7.

scribed in most realistic ocean general circulation models as a salinity relaxation toward an observed climatological state (Bryan and Holland 1989; Beckman et al. 1994). Unless the model is able to reproduce the observed gyre boundaries and their associated salinity fronts, this relaxation likely induces anomalous freshwater fluxes that may be important in the jet separation process. The importance of the freshwater flux prescription was also pointed out recently by Huang and Schmitt (1993) and Huang (1993), who showed that the mass flux at the ocean surface due to $E - P$ can actually induce a barotropic flow in the interior sufficient to cause a southward shift of the separation point of the Gulf Stream of the order of 100 km.

Furthermore, in a numerical study of the variability and the separation of the Gulf Stream induced by surface atmospheric forcing and lateral boundary flows, Ezer and Mellor (1992) conclude that diabatic pro-

cesses are essential in maintaining the density structure and the associated geostrophic flow in the northern recirculation gyre and that such processes play an important role in the separation. Maintenance of the density structure in their model is achieved by a balance among heat transfer, wind stress, and slope water inflow and is primarily a diabatic process (i.e., as opposed to a potential vorticity conserving lateral water mass redistribution process). In their view, potential vorticity conservation theories of the separation do not explain maintenance of the Gulf Stream path. Their model has a bottom-following vertical coordinate, realistic topography, and open boundary conditions. It is a regional model that, in contrast to a basin-scale model, is greatly affected by the prescribed open boundary conditions.

In summary, the separation point of the midlatitude jet is no longer south of the ZWCL, as in the Parsons (1969) adiabatic outcropping mechanism, when diabatic processes are taken into account. The underlying layers outcrop into the mixed layer where the horizontal density gradient is a maximum. The maintenance of this maximum results from a balance between potential vorticity conservation (mechanical forcing) and thermal processes. This is in agreement with Veronis (1978), who concludes that separation of western boundary currents from the coasts is determined by the intensity of the thermal driving as well as by the wind stresses. Additional effects not discussed in this paper such as the deep sinking of cold water at northern latitudes are also likely to be of importance. Finally, in most of the experiments presented in this paper, the separation latitude is at the ZWCL. It may be of interest to relate this to the fact that the axis of the climatological zero wind stress curl in the Atlantic (e.g., Hellerman and Rosenstein 1983; COADS) overlays the Gulf Stream extension.

*Acknowledgments.* Discussions with G. Veronis proved timely and valuable. We also would like to thank J. Wang for his assistance with the two-layer simulations. Support was provided by the National Science Foundation through Grant OCE-9102560 and by the Office of Naval Research under Contract N00014-93-1-0404. Computations were carried out using the CRAY Y-MP at the National Center for Atmospheric Research (NCAR). NCAR is sponsored by the National Science Foundation.

## REFERENCES

Beckmann, A., C. W. Böning, C. Köberle, and J. Willebrand, 1994: Effects of increased horizontal resolution in a simulation of the North Atlantic Ocean. *J. Phys. Oceanogr.*, **24,** 326–344.

Bleck, R., and D. B. Boudra, 1986: Wind-driven spin up in eddy-resolving ocean models formulated in isopycnic and isobaric coordinates. *J. Geophys. Res.*, **91,** 7611–7621.

——, and E. P. Chassignet, 1994: Simulating the oceanic circulation with isopycnic-coordinate models. *The Oceans: Physical-Chemical Dynamics and Human Impact.* S. K. Majumdar, E. W. Miller, G. S. Forbes, R. F. Schmalz, and A. A. Panah, Eds., The Pennsylvania Academy of Science, 17–39.

——, H. P. Hanson, D. Hu, and E. B. Kraus, 1989: Mixed layer/thermocline interaction in a three-dimensional isopycnal model. *J. Phys. Oceanogr.*, **19,** 1417–1439.

——, C. Rooth, D. Hu, and L. T. Smith, 1992: Salinity-driven transients in a wind- and thermohaline-forced isopycnic coordinate model of the North Atlantic. *J. Phys. Oceanogr.*, **22,** 1486–1505.

Bryan, F. O., and W. R. Holland, 1989: A high resolution simulation of the wind- and thermohaline-driven circulation in the North Atlantic Ocean. *Parameterization of Small-Scale Processes. Proceedings Aha Huliko'a Hawaiian Winter Workshop.* P. Muller and D. Anderson, Eds., University of Hawaii, 99–115.

Cessi, P., 1991: Laminar separation of colliding western boundary currents. *J. Mar. Res.*, **49,** 697–717.

Chassignet, E. P., 1995: Vorticity dissipation by western boundary currents in the presence of outcropping layers. *J. Phys. Oceanogr.*, **95,** 242–255.

——, and P. R. Gent, 1991: The influence of boundary conditions on midlatitude jet separation in ocean numerical models. *J. Phys. Oceanogr.*, **21,** 1290–1299.

——, and R. Bleck, 1993: The influence of layer outcropping on the separation of boundary currents. Part I: The wind-driven experiments. *J. Phys. Oceanogr.*, **23,** 1485–1507.

Ezer, T., and G. L. Mellor, 1992: A numerical study of the variability and the separation of the Gulf Stream, induced by surface atmospheric forcing and lateral boundary flows. *J. Phys. Oceanogr.*, **22,** 660–682.

Gangopadhyay, A., P. Cornillon, and D. R. Watts, 1992: A test of the Parsons–Veronis hypothesis on the separation of the Gulf Stream. *J. Phys. Oceanogr.*, **22,** 1286–1301.

Haidvogel, D. B., J. C. McWilliams, and P. R. Gent, 1992: Boundary current separation in a quasigeostrophic, eddy-resolving ocean circulation model. *J. Phys. Oceanogr.*, **22,** 882–902.

Hellerman, S., and M. Rosenstein, 1983: Normal monthly wind stress over the World Ocean with error estimates. *J. Phys. Oceanogr.*, **13,** 1093–1104.

Han, Y.-J., 1984: A numerical World Ocean general circulation model. Part II: A baroclinic experiment. *Dyn. Atmos. Oceans,* **8,** 141–172.

Haney, R. L., 1971: Surface thermal boundary condition for ocean circulation models. *J. Phys. Oceanogr.*, **1,** 241–248.

Huang, R. X., 1993: Real freshwater flux as a natural boundary condition for the salinity balance and thermohaline circulation forced by evaporation and precipitation. *J. Phys. Oceanogr.*, **23,** 2428–2446.

——, and G. Flierl, 1987: Two-layer models for the thermocline and current structure in subtropical/subpolar gyres. *J. Phys. Oceanogr.*, **17,** 872–884.

——, and R. W. Schmitt, 1993: The Goldsborough–Stommel circulation of the World Oceans. *J. Phys. Oceanogr.*, **23,** 1277–1284.

Kamenkovich, V. M., and G. M. Reznik, 1972: A contribution to the theory of stationary wind-driven currents in a two-layer liquid. *Izv. Acad. Sci. USSR, Atmos. Oceanic. Phys.*, **8,** 238–245.

Lamb, P. J., and A. F. Bunker, 1982: The annual march of the heat budget of the North and Tropical Atlantic Ocean. *J. Phys. Oceanogr.*, **12,** 1388–1410.

Ledwell, J. R., A. J. Watson, and C. S. Law, 1993: Evidence for slow mixing across the pycnocline from an open-ocean tracer-release experiment. *Nature,* **364,** 701–703.

Levitus, S., 1982: *Climatological Atlas of the World Ocean.* NOAA Prof. Paper No. 13, U.S. Govt. Printing Office, 173 pp.

Nurser, A. J. G., and R. G. Williams, 1990: Cooling Parsons's model of the separated Gulf Stream. *J. Phys. Oceanogr.*, **20,** 1974–1979.

Parsons, A. T., 1969: A two-layer model of Gulf Stream separation. *J. Fluid Mech.*, **39,** 511–528.

Pedlosky, J., 1987: On Parsons' model of the ocean circulation. *J. Phys. Oceanogr.*, **17,** 1571–1582.

Schmitt, R. W., P. S. Bogden, and C. E. Dorman, 1989: Evaporation minus precipitation and density fluxes for the North Atlantic. *J. Phys. Oceanogr.*, **19,** 1208–1221.

Smolarkiewicz, P., 1984: A fully multidimensional positive definite advection transport algorithm with small implicit diffusion. *J. Comput. Phys.*, **54,** 325–362.

Stommel, H., 1960: *The Gulf Stream: A Physical and Dynamical Description.* 2d ed. University of California Press, 202 pp.

Sun, S., R. Bleck, and E. P. Chassignet, 1993: Layer outcropping in numerical models of stratified flows. *J. Phys. Oceanogr.*, **23,** 1877–1884.

Thompson, J. D., and W. J. Schmitz, 1989: A limited-area model of the Gulf Stream: Design, initial experiments, and model-data intercomparison. *J. Phys. Oceanogr.*, **19,** 791–814.

Veronis, G., 1973: Model of World Ocean circulation. Part I: Wind-driven, two-layer. *J. Mar. Res.*, **31,** 228–288.

——, 1976: Model of World Ocean circulation. Part II: Thermally-driven two-layer. *J. Mar. Res.*, **34,** 199–216.

——, 1978: Model of World Ocean circulation. Part III: Thermally and wind-driven. *J. Mar. Res.*, **36,** 1–44.

——, 1981: Dynamics of large-scale ocean circulation. *Evolution of Physical Oceanography,* B. A. Warren and C. Wunsch, Eds., The MIT Press, 140–183.

Verron, J., and C. LeProvost, 1991: Response of eddy-resolved general circulation models to asymmetrical wind forcing. *Dyn. Atmos. Oceans,* **15,** 505–533.